



Efficient photodegradation of acid orange 7 by using ultrasound-assisted synthesis of ternary graphene nanocomposite based on TiO₂

Farnosh Tavakoli^{a,b}, Alireza Badiei^{a,*}, Masoud Salavati Niasari^c

^aSchool of Chemistry, College of Science, University of Tehran, Tehran, Iran, email: abadiei@khayam.ut.ac.ir

^bYoung Researchers and Elite Club, Kazerun branch, Islamic Azad University, Kazerun, Iran

^cInstitute of Nano Science and Nano Technology, University of Kashan, Kashan, Iran

Received 4 June 2018; Accepted 31 October 2018

ABSTRACT

Herein, we were synthesized AgI-TiO₂-graphene (G) nanocomposite photocatalyst by sonochemical method. The nanocomposites of AgI-TiO₂-G, TiO₂-G, and AgI-G and the hybrid of AgI-TiO₂ were analyzed using X-ray diffraction, field emission scanning electron microscopy, transmission electron microscopy, energy dispersive X-ray spectroscopy, diffuse reflectance spectroscopy, photoluminescence, and fourier-transform infrared spectroscopy. The AgI-TiO₂-G composite possessed high photocatalytic properties. The ternary composite with 4 wt% TiO₂ and 50 wt% AgI showed enhanced photocatalytic degradation (90%) compared with that of pure graphene (36%), AgI-TiO₂ (85%), bare TiO₂ (61%), AgI (53%), TiO₂-G (84%), and AgI-G (81%). According to the results, ultrasound irradiation had crucial effect on quality of nanoparticles and graphene sheets. The photocatalytic performances of all photocatalyst compounds were studied on decomposition of acid orange 7.

Keywords: Ultrasonic; Nanocomposites; Degradation; Photocatalytic activity; TiO₂

1. Introduction

Water is essential to life. It is especially necessary to the human beings, first for his food, then for his health, and finally for his agricultural and industrial activities. Clean water ensures the survival of human life. For the degradation of the organic pollutants effectively, the photocatalysts based on TiO₂ are very effective and have attracted researchers in recent years. On the other hand, graphene, a two-dimensional graphitic compound, is a material with extraordinary properties [1,2]. It should be noted that the nanoparticles are directly decorated on the graphene sheets without any molecular linkers. Therefore, many types of nanoparticles can be deposited on the graphene sheets and create interesting applications such as catalytic, energy storage, photocatalytic, and optoelectronic applications [3]. There are various methods for the synthesis of graphene

composites, including pre-graphenization, post-graphenization, and syn-graphenization [4,5].

The TiO₂ nanoparticles have been used for photocatalytic elimination of dyes due to their extraordinary optical properties [6–8]. The photocatalytic degradation mechanism of TiO₂ nanoparticles has been proven [9,10]. One of the TiO₂ problems is the recombination of electrons and holes [11]. But graphene can solve this problem in TiO₂ with its amazing electron mobility and large surface area. On the other hand, graphene can act as an efficient transmitter and acceptor electron to improve photoinduced charge transfer; therefore, it can inhibit the recombination of the photogenerated electron-holes [12]. Recently, Lightcap et al [13] showed that TiO₂-graphene (G) composite shows high performance for photodegradation of methylene blue. Xu et al [14] pointed out that the TiO₂-G composite was a highly efficient photocatalyst for the elimination of benzene in gas phase. Dai et al [15] reported a TiO₂-G composite prepared by growing TiO₂ nanocrystals on graphene oxide (GO) through hydrolysis of Ti(BuO)₄ for photodegradation activity of TiO₂ to decomposed rhodamine B. Recently, Cui and co-workers

* Corresponding author.

[16] prepared the TiO₂-G and showed higher photocatalytic activity for H₂ evolution. Moreover, AgI nanoparticles show high photocatalytic performance [17,18]. In order to further increase the photocatalytic activity of TiO₂-G composite, silver and silver halide have been used [19–21].

Here, AgI-TiO₂-G composite was prepared by using ultrasound irradiation. This ternary composite was used for photodegradation of acid orange 7 (AO7) as a pollutant model. In order to check the presence of graphene, TiO₂ and AgI nanostructures in photodegradation performance of AO7, AgI-TiO₂, AgI-G, and TiO₂-G composites were synthesized and characterized. On the other hand, the weight ratios of TiO₂ and AgI to graphene in composites of TiO₂-G and AgI-G as crucial effects on photodegradation performance were investigated. Finally, the effect of ultrasound irradiation on photocatalytic performance of ternary composite was examined.

2. Materials and methods

2.1. Synthesis of TiO₂-G

A typical procedure for the synthesis of TiO₂-G nanocomposite is as follows: 0.2 g graphite oxide was dispersed in 10 mL water for 15 min under ultrasound irradiation. Then a solution containing 0.02 g TiO₂ in 10 mL of water was added slowly into above mixture. After hydrothermal reaction at 80°C for 5 h, GO was reduced to graphene nanosheets and TiO₂ nanoparticles were fixed on its surface to generate a TiO₂-G composite. Finally, the resulting mixture was centrifuged, and the precipitate was dried at 60°C. After drying at 60°C for 8 h, the TiO₂-G composite was obtained. In order to study the effect of different weight ratios of TiO₂ in as-synthesized composite, seven different weight ratios of TiO₂ to the graphene (1, 2, 3, 4, 10, 12.5, and 25 wt%) were prepared.

2.2. Synthesis of AgI-G

For synthesis of AgI-G nanocomposite, 0.1 g graphite oxide was dispersed in 10 mL of water for 15 min under ultrasound irradiation. Then a solution containing 0.1 g AgNO₃ in 10 mL of water was added slowly into the above mixture. The as-obtained mixture was stirred under magnetic stirring for 2 h to produce a uniform precipitate. A 0.1 g KI was added under ultrasound irradiation for 15 min. After hydrothermal reaction at 80°C for 5 h, the GO was reduced to graphene nanosheets and AgI nanoparticles were grown on its surface to generate AgI-G composite. Finally, the resulting mixture was centrifuged, and the precipitate was dried at 60°C. The obtained solid was collected and washed with distilled water. After drying at 60°C for 8 h, the AgI-G with different weight ratios of AgI (25, 37.5, 50, and 75 wt%) were obtained.

2.3. Synthesis of TiO₂-AgI-G

For synthesis of TiO₂-AgI-G, 0.1 g graphite oxide was dispersed in 10 mL of water for 15 min under ultrasound irradiation. Then, a solution containing 0.008 g TiO₂ powder in 10 mL of water was added dropwise into the above mixture.

After that 0.15 g AgNO₃ was added to the mixture, and in the next stage, 1 mmol KI was added. At this point, TiO₂ and AgI are formed on the surface of graphene. Finally, the mixture was cooled down in room temperature and filtered. The obtained solid was collected and washed several times with distilled water. After drying at 60°C for 8 h, the TiO₂-AgI-G composite was obtained.

3. Results and discussion

3.1. Characterization of nanocomposites

Fig. 1 shows the SEM images of graphene, TiO₂, AgI, AgI-G, and AgI-TiO₂-G composite. As shown in Fig. 1(a), graphene nanosheets are individually exfoliated. According to Fig. 1(b), spherical morphology of TiO₂ is shown. Fig. 1(c) shows the SEM image of the TiO₂-G composite that TiO₂ nanoparticles were observed on the graphene sheets. SEM images of AgI nanoparticles and AgI-G composite are shown in Fig. 1(d) and (e), respectively. As mentioned above for TiO₂-G composite, in the case of AgI-G composite, AgI nanoparticles are well dispersed on the surface of graphene. SEM image of ternary AgI-TiO₂-G composite is shown in Fig. 1(f) and that TiO₂ and AgI nanoparticles are well distributed on graphene sheets.

Transmission electron microscopy (TEM) images of graphene and AgI-TiO₂-G composite are shown in Fig. 2. According to TEM images, AgI and TiO₂ particles are mounted on the graphene sheet surfaces and some particles intercalate between the graphene interlayer.

Fig. 3 shows the diffuse reflectance spectroscopy (DRS) spectra of TiO₂, AgI, AgI-TiO₂, and AgI-TiO₂-G composite. According to Fig. 4, the calculated bandgap energies of TiO₂, AgI, AgI-TiO₂, and AgI-TiO₂-G are 3.24, 2.38, 2.80, and 2.65 eV, respectively. The slightly reduced bandgap of AgI-TiO₂-G composite implies that unpaired π electrons from graphene may bond with free electrons of TiO₂ [22].

The valence band (VB) and conduction band (CB) potential edges were calculated using the below formula [23,24]:

$$E_{\text{VB}} = X - E^e + 0.5(E_g) \quad (1)$$

$$E_{\text{CB}} = E_{\text{VB}} - E_g \quad (2)$$

where E_{VB} and E_{CB} are the VB and CB edge potentials of a semiconductor, respectively. X is the electronegativity value of the semiconductor, E^e is the free electrons on the hydrogen scale energy (~4.5 eV), and E_g is the band gap energy of the semiconductor compound. The calculated VB potentials of TiO₂ and AgI are 2.95 and 2.38 eV, respectively. The CB potential of TiO₂ (-0.29 eV) is lower than the CB of AgI (-0.42 eV). So, the photogenerated electrons in the AgI move to TiO₂ through interfaces. The presence of graphene on ternary composite influences the recombination of electrons and holes. So, according to delays on recombination processes, the photodegradation performance of ternary composite was increased.

Fig. 4 shows the X-ray diffraction (XRD) patterns of AgI, AgI-TiO₂-G, GO, and TiO₂. The diffractogram of GO exhibited the typical reflections at $2\theta = 26.48^\circ$ and 43.17°

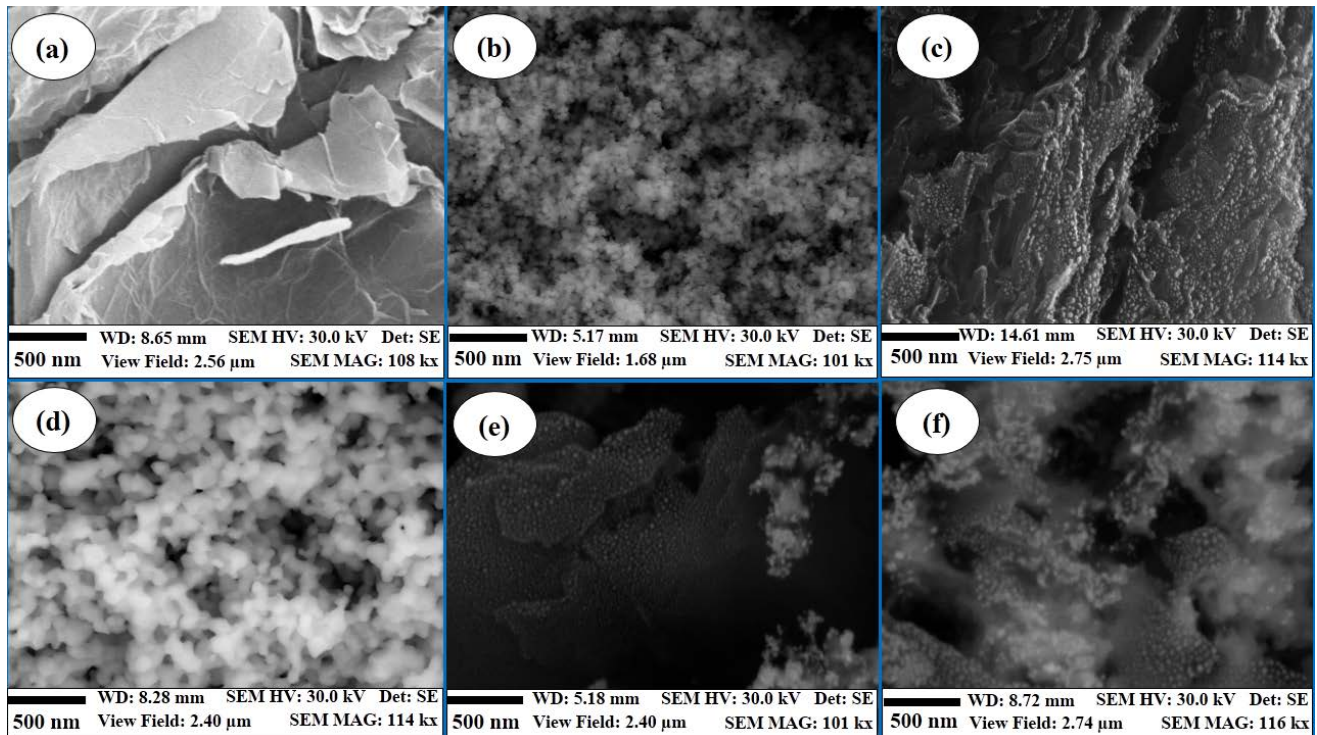


Fig. 1. SEM images of (a) graphene, (b) TiO_2 , (c) TiO_2 -G, (d) AgI, (e) AgI-G, and (f) AgI- TiO_2 -G.

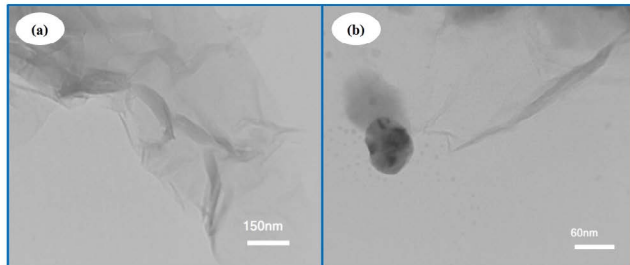


Fig. 2. TEM images of (a) graphene and (b) AgI- TiO_2 -G.

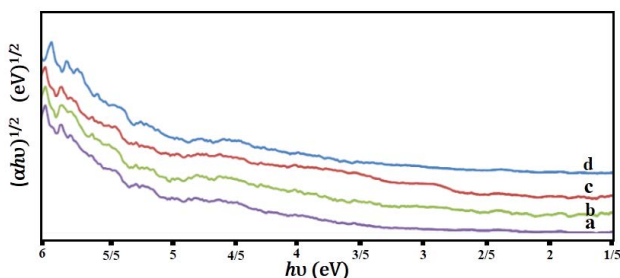


Fig. 3. DRS of (a) TiO_2 , (b) AgI, (c) AgI- TiO_2 , and (d) AgI- TiO_2 -G.

corresponding to the (002) and (100) reflections (JCPDS 01-0646) (Fig. 4(c)). According to Fig. 5(d) for the TiO_2 compound, the XRD reflections at 2θ of 25.8° , 38° , 39.5° , 48° , 55° , 62.6° , 69.7° , and 75.7° can be indexed to the characteristic reflections of the (101), (004), (112), (200), (211), (213), (220), and (215) plane reflections of anatase crystal structure TiO_2 , respectively. For the TiO_2 -AgI-G composite, the (002) and

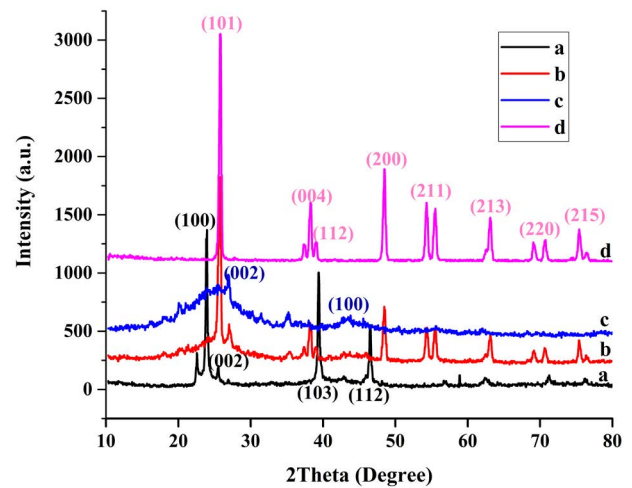


Fig. 4. XRD patterns of (a) AgI, (b) AgI- TiO_2 -G, (c) GO, and (d) TiO_2 .

(100) reflections of graphene overlapped the anatase (200) and (113) reflections of TiO_2 . Therefore, the intensity of the reflection at $2\theta = 25.8^\circ$ from the AgI- TiO_2 -G composite was stronger than that from the TiO_2 compound. On the other hand, the AgI nanoparticles give the diffraction patterns at 22.6° , 24.43° , 41° , and 46.6° which correspond to (100), (002), (103), and (112) planes, which could be attributed to β -AgI structure (JCPDS 78-1614) (Fig. 4(a)). No peak for GO or impurities was detected in XRD patterns of AgI- TiO_2 -G (Fig. 4(b)). It is also very difficult to distinguish the diffraction pattern of GO from the broader (101) plane of anatase TiO_2 . Based on the XRD pattern of AgI- TiO_2 -G composite, all the

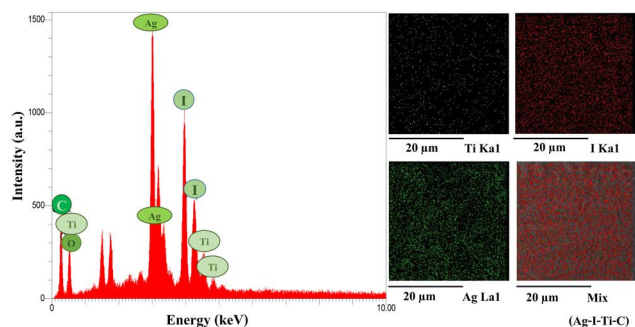


Fig. 5. EDX spectrum of AgI-TiO₂-G composites and its elemental mapping images.

reflections of AgI and TiO₂ nanoparticles are observed in XRD patterns of ternary composite.

To get information on the elements, the AgI-TiO₂-G composite was examined by EDX analysis. Fig. 5 shows the EDX analysis of the AgI-TiO₂-G composite. According to this spectrum, the lines that attributed to Ag, I, Ti, O, and C are obviously observed. Results confirmed the existence of AgI and TiO₂ nanoparticles on the surface of graphene. AgI and TiO₂ being present on the graphene surface emerged to trap the migrated electron (e^-), leaving the holes (h^+) free to react with water molecules to form hydroxyl radicals.

Fig. 6 shows the photoluminescence spectra of the as-synthesized samples measured by an excitation wavelength of 320 nm at room temperature. PL peaks were observed at about 358 and 398 nm for all samples, which correspond to the direct recombination between photo-generated electron-hole pairs. This result indicates that the AgI-TiO₂-G composite has higher photocatalytic activities as compared with that of others.

The Brunauer-Emmet-Teller (BET) surface area and pore structure have crucial effect on the photocatalytic performance of photocatalysts. Fig. 7 shows the nitrogen adsorption-desorption isotherms and the corresponding pore size distribution curves of GO and AgI-TiO₂-G composite. The nitrogen adsorption-desorption curves of these samples indicate the presence of micropores. The results of BET surface area and average pore size of GO and AgI-TiO₂-G are

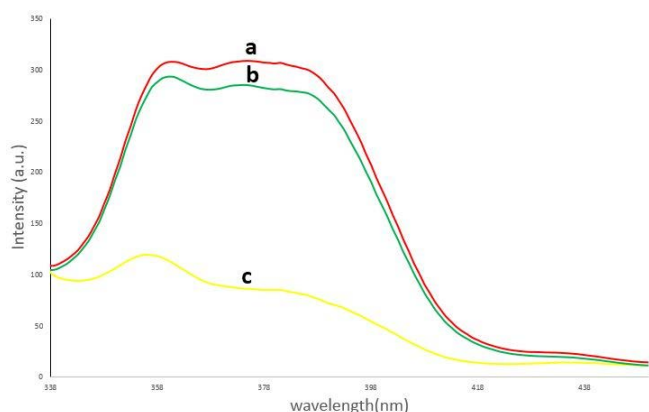


Fig. 6. PL spectrum of (a) TiO₂, (b) TiO₂-G, and (c) AgI-TiO₂-G.

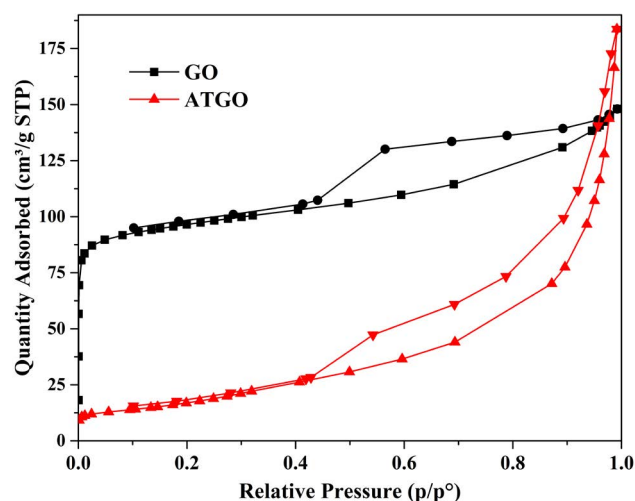


Fig. 7. Nitrogen adsorption-desorption isotherms of GO and AgI-TiO₂-G (ATGO).

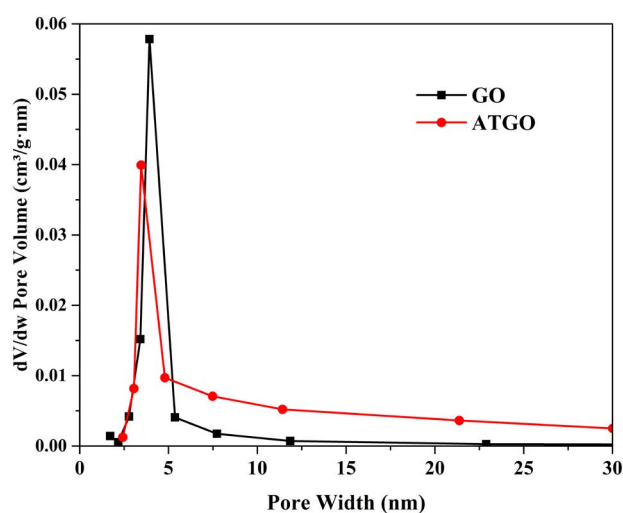


Fig. 8. Pore size distribution of Go and AgI-TiO₂-G (ATGO).

shown in Figs. 7 and 8. According to the results, the specific surface area of GO (303.96 m²/g) decreases after placement of AgI and TiO₂ on the surface of graphene in AgI-TiO₂-G nanocomposite (64.36 m²/g).

Fig. 9 shows the Raman spectrum of GO and AgI-TiO₂-G nanocomposite. It is well known that Raman spectroscopy is a powerful method for the characterization of sp² and sp³ hybridized carbon atoms in graphene to distinguish the ordered and disordered/defect structures. Therefore, the Raman spectroscopy of GO and AgI-TiO₂-G nanocomposite was carried out (Fig. 9). The two characteristic peaks of GO can be found at 1350 and 1585 cm⁻¹ corresponding to the D and G bands, respectively. For the AgI-TiO₂-G composite, we observed the characteristic band of composite at 68 cm⁻¹ as well as the D band (1350 cm⁻¹) and G band (1585 cm⁻¹) of GO, suggesting that the structure of GO is maintained in AgI-TiO₂-G nanocomposite. The intensity of ratio of D band to G band can estimate the degree of disorder/defects in graphene. The increase of I_D/I_G is attributed to the reduction

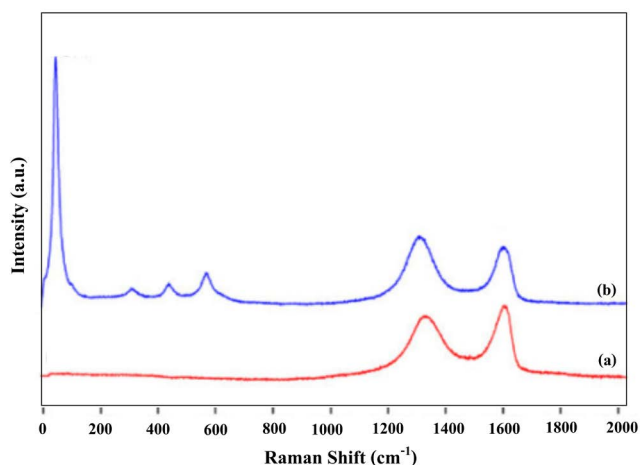


Fig. 9. Raman spectrum of (a) graphene oxide and (b) AgI-TiO₂-G nanocomposite. (Takram Raman spectrometer 532 nm).

and restoration of the sp² network of GO during the reduction process and the formation of more defects in GO.

3.2. How to connect TiO₂ and AgI to graphene surface

Since the synthesis procedure of AgI-TiO₂-G was post-graphenization, we used GO for the synthesis of AgI-TiO₂-G composite. Because GO is a hydrophilic compound due to presence of oxygen functional group on its surface, this combination is well dispersible in water. On the other hand, TiO₂ is a hydrophilic compound that can connect to graphene surface via hydrogen bond to oxygen groups. As mentioned in the experimental part, AgI and TiO₂ nanoparticles were placed on the graphene surface but, since AgI is a hydrophobic nanoparticle, cannot connect to GO directly. So, AgI connects to TiO₂ and TiO₂ as a hydrophobic nanoparticle connects to oxygen functional groups of GO. So, TiO₂ as a hydrophilic compound can act as a linker between AgI and GO. As shown in SEM images of AgI, TiO₂, and AgI-TiO₂-G, spherical TiO₂ nanoparticles connect to amorphous AgI nanoparticles and then these two nanoparticles are placed on the surface of GO. According to TEM image, both spherical TiO₂ and amorphous AgI nanoparticles are placed on the graphene surface.

3.3. Effect of ultrasound wave on photocatalytic performance

To show the specific role of ultrasound on the photocatalytic degradation activity, AgI-TiO₂-G photocatalyst was prepared without ultrasound and the photodegradation was carried out using AO7. A blank test was done without sonication at temperature of about 50°C with vigorous magnetic stirring for 20 min by using AgNO₃, KI, TiO₂, and graphene as starting reagents. Since the reaction temperature increased from room temperature to 50°C after sonication for 20 min, the blank test was repeated at 50°C under magnetic stirring for 20 min. SEM image of the blank sample is shown in Fig. 10(a). In the presence of ultrasound irradiation, the graphene sheets with nanosized particles were produced, whereas microsized structures with high agglomeration were formed [25,26]. It is known that the physical effects of ultrasound can influence

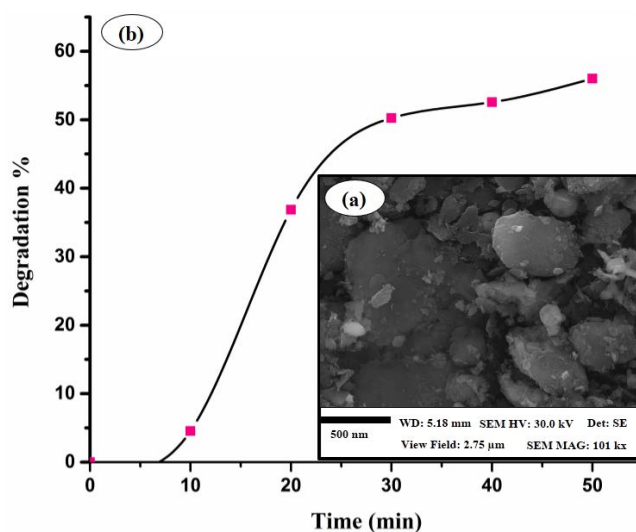


Fig. 10. (a) SEM image of blank sample, and (b) degradation spectra of AO7 using blank sample.

the properties of materials [27]. As it is shown in Fig. 10(b), the photocatalyst prepared without ultrasound irradiation exhibits only 56% photodegradation, whereas the photocatalyst prepared in the presence of ultrasound irradiation shows 90% of AO7 degradation. Ultrasound-assisted synthesis of composites helps to increase the surface active sites of the photocatalysts due to the reduction of TiO₂ and AgI particle sizes [22,28]. According to Fig. 10(b), ultrasound irradiation is an important factor for the enhancement in photodegradation of dye molecules. On the other hand, shear forces of ultrasound enhance uniform distribution and loading of TiO₂ and AgI nanoparticles on the surface of graphene sheets which is clearly seen from field emission scanning electron microscopy (FESEM) images (Fig. 1). Therefore, this result shows that during the synthesis of nanomaterials, ultrasound irradiation plays an important role for increasing the photocatalyst performance.

3.4. Photocatalytic performance of nanocomposites

The photocatalytic performances of the AgI, TiO₂, TiO₂-G, AgI-G, and AgI-TiO₂-G were investigated using aqueous AO7 dye as a model compound under UV light irradiation. The adsorption of pollutants on catalyst surface is a crucial factor for the degradation of dyes [29]. Compared with AgI-TiO₂, the AgI-TiO₂-G composite shows higher adsorption of dye molecules (Fig. 11(a)). This higher photocatalytic activity of composite based on graphene was due to the increased adsorptivity of compound.

As shown in Fig. 11(a), when only AO7 dye was exposed to UV light, no degradation of AO7 was observed. According to this observation, degradation of AO7 is only dependent on photocatalyst.

3.5. Photocatalytic performance of TiO₂-G nanocomposite

In order to study the effect of TiO₂ loading, different weight ratios of TiO₂ (1, 2, 3, 4, 10, 12.5, and 25 wt%)-loaded graphene photocatalyst were prepared and their

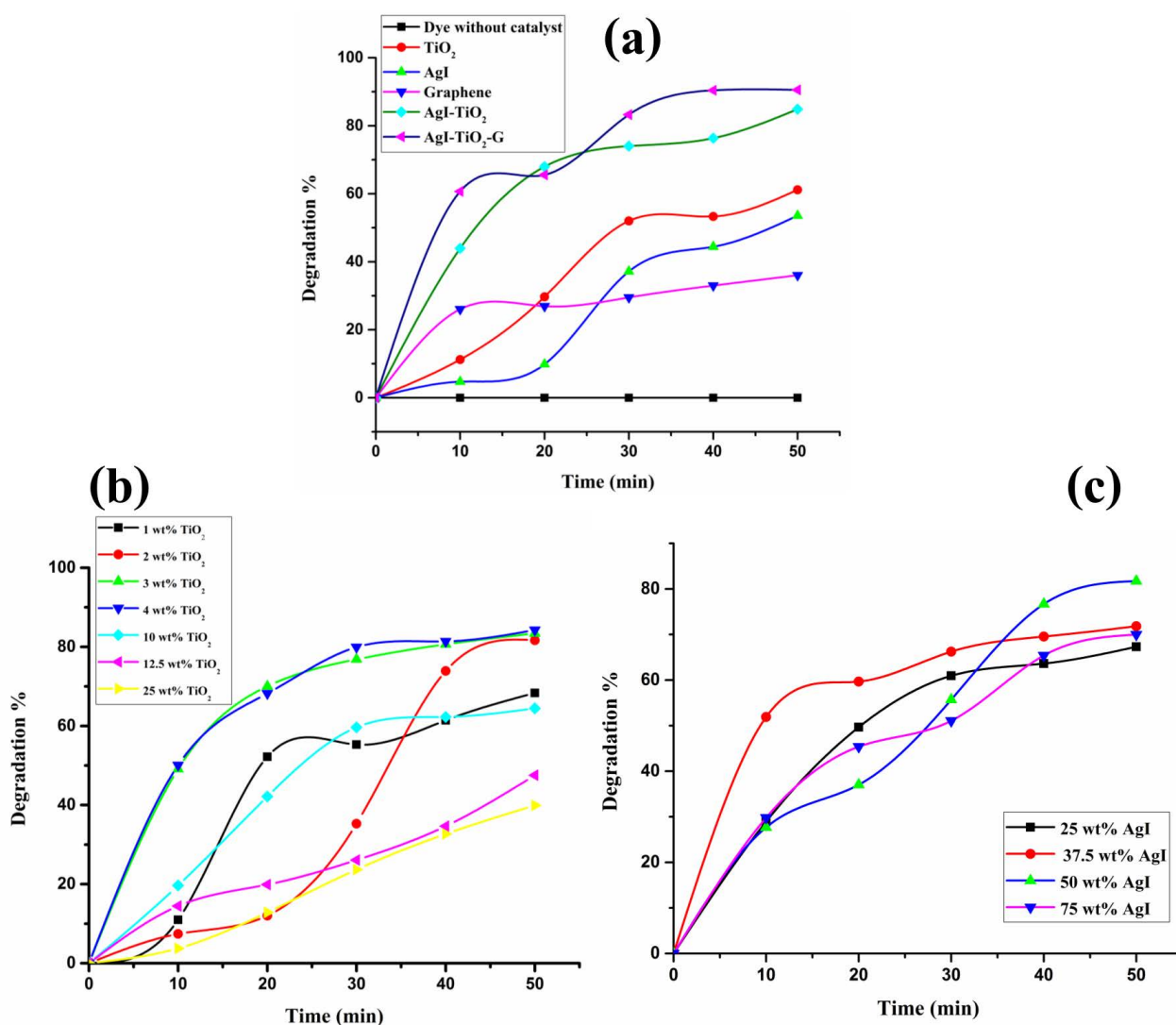


Fig. 11. Degradation curve of AO7 aqueous dye with (a) UV light without photocatalyst, TiO₂, AgI, graphene, AgI-TiO₂ and ternary composite; (b) different weight ratio of TiO₂ to graphene and (c) different weight ratio of AgI to graphene.

photocatalytic performance was also tested (Fig. 11(b)). The composite with 4 wt% TiO₂ showed higher photocatalytic degradation compared with pure graphene and bare TiO₂ nanoparticle, while 12.5 and 25 wt% TiO₂-loaded graphene photocatalyst decreased the photocatalytic activity. As shown in Fig. 11(b), by increasing the weight ratio of TiO₂ to graphene, the photodegradation performance of composite for AO7 was decreased; the first reason for decreasing the photodegradation is that higher loading of TiO₂ could increase the recombination rate of electrons and holes, thereby preventing the separation of charges. The second reason is that higher loading of TiO₂ may decrease the surface area of graphene and adsorptivity of graphene for adsorbing dye molecules on the surface of graphene and thereby influencing the photocatalytic performance and so preventing the light to reach active sites of composites. According to Fig. 11(b), graphene with 4 wt% TiO₂ exhibits 84% AO7 degradation within 50 min but only 61% and 36% of degradation in the presence of bare TiO₂ and graphene, respectively. This

increase in photodegradation of dye molecules is due to overlapping of the CBs of TiO₂ and graphene resulting in an effective separation of charge carrier between graphene and the TiO₂ interface. Since 4 wt% TiO₂-loaded graphene was found to show an optimum efficiency, AgI-TiO₂-G composite was synthesized with 4 wt% TiO₂-loaded AgI-G photocatalyst.

3.6. Photocatalytic performance of AgI-G nanocomposite

In order to investigate the optimum weight ratio of AgI loaded in graphene, 5 different weight ratios of AgI were used and the best weight ratio was selected to synthesize AgI-TiO₂-G composite with the optimum weight ratio of AgI in terms of photocatalytic performance. As shown in Fig. 11(c), the AgI-G composite with 50 wt% AgI showed enhanced photocatalytic degradation compared with that of pure graphene and bare AgI nanoparticle, while 25, 37.5, and 75 wt% AgI-loaded graphene photocatalyst decreased the photocatalytic activity than the composite with 50 wt%

AgI. Increasing the recombination rate and low specific surface area are the reasons that could decrease the photocatalytic activity of AgI-G composite with higher weight ratio of AgI which is greater than 50 wt% of AgI nanoparticles. It can be seen in Fig. 11(c) that AgI-G photocatalyst with 50 wt% AgI exhibits 81% AO7 degradation within 50 min but only 53% and 36% of degradation observed by AgI and graphene, respectively.

3.7. Photocatalytic performance of AgI-TiO₂ nanostructure and AgI-TiO₂-G nanocomposite

In order to check the effect of graphene loading, AgI-TiO₂ photocatalyst was synthesized and its photocatalytic efficiency was tested under UV light. Based on Fig. 11(a), in presence of AgI-TiO₂ composite 79% degradation was shown in AO7 dye, whereas graphene-loaded AgI-TiO₂ composite exhibits 90% AO7 photodegradation within 50 min increased the AO7 degradation was observed due to increasing adsorption and surface area those are related to presence of graphene in the composites. The other effective factor in increasing degradation of AO7 is the formation of π - π links between pollutants and aromatic rings of graphene. Formation of ionic interactions between dye molecules and oxygen-containing functional groups of graphene is the next key factor that plays a crucial role in the degradation of dyes. Generally, graphene plays the roles of adsorbent and electron acceptor.

3.8. Photocatalytic mechanism

Hydroxyl radicals (OH), superoxide anions (O₂⁻), and holes (h⁺) are the reactive species for the photocatalytic process. In order to understand the photocatalytic activity of AgI-TiO₂-G composite, benzoic acid (as an OH radical scavenger), EDTA (as a h⁺ scavenger), and Ar gas (as an inert gas that prevents the presence of O₂ molecules thereby prevents the formation of O₂⁻) were applied as shown in Fig. 12. In the presence of benzoic acid (0.5 mM), 10 mL EDTA (0.01M), and Ar gas, 72%, 85%, and 61% degradations were observed, respectively. In the presence of benzoic acid, EDTA, and Ar gas, 18%, 5%, and 29% degradations were decreased than that of the scavenger-free photocatalytic system for AO7, as shown in Fig. 12. OH and O₂⁻ anions are responsible for the photodegradation of AO7.

The possible degradation proposed photocatalytic mechanism of AO7 degradation over graphene-supported photocatalyst is illustrated in Fig. 13. When AgI-TiO₂-G was irradiated with UV light, electrons from the VB of AgI are excited to the CB of AgI so holes are created in the valence bond. According to the energy level position of AgI and TiO₂, electrons move from AgI (CB) to TiO₂ (CB). Since the CB work function of TiO₂ matches with CB work function of graphene [30–36], electrons can be easily transferred from CB of TiO₂ to graphene. As a result, the oxygen sites can readily accept the electrons and carry out the reduction reaction to generate more superoxide radicals. Due to the presence of electrons on the sheets of graphene in photocatalysts, excess amounts of reactive O₂⁻ radicals are produced. Therefore, the transportation of photogenerated electrons over graphene sheet can reduce O₂ to O₂⁻ radicals which enhanced AO7 degradation. As discussed above, degradation of AO7 is done not only

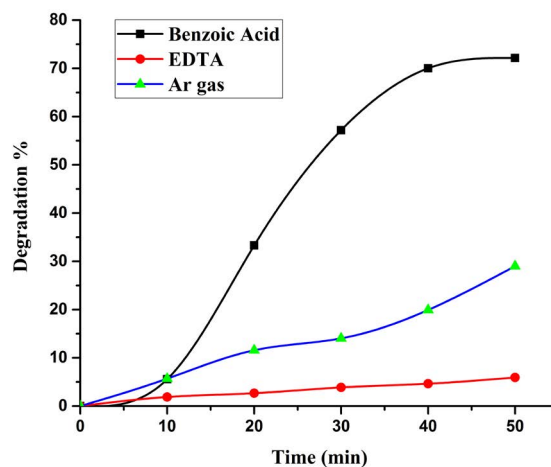


Fig. 12. A series of trapping experiments (Benzoic Acid, EDTA and Ar gas) for the degradation of AO7 over AgI-TiO₂-G photocatalysts under UV light irradiation.

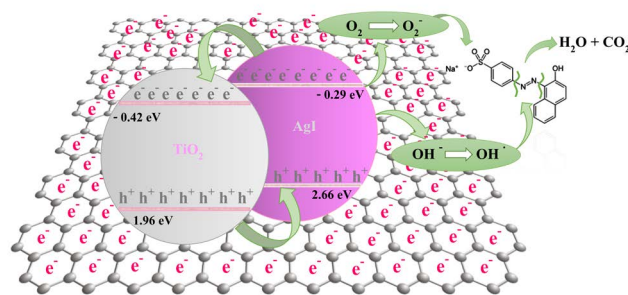
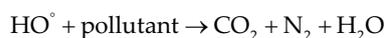
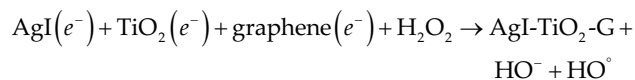
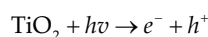


Fig. 13. The possible photocatalytic mechanism of AO7 degradation over AgI-TiO₂-G composite.

through the O₂⁻ but also through the h⁺. The mechanism for the decomposition of AO7 by AgI-TiO₂-G is as follows:



3.9. Formation mechanism of AgI-TiO₂-G nanocomposite

Ultrasound waves radiate through the solution making millions of micro- and nanosized bubbles, and these grow in

the low-pressure stage and subsequently collapse violently in the high-pressure stage. The collapsing bubbles generate microjets and shockwaves that lead to pressures reaching hundreds or thousands of atmospheres. The energy released from this process, known as acoustic cavitation, can accelerate the rate of chemical reactions. In this work, AgI-TiO₂-G nanocomposites have been synthesized by using AgNO₃, KI, GO, and TiO₂ powders in the presence of ultrasound irradiation. We can assume that Ag⁺ ions in the solution combine with iodide ions to yield AgI species. Among the radicals generated in the sonolysis of water molecules under the air atmosphere, H[•], OH[•], O₂^{-•}, and HO₂[•] radicals are known to participate in the synthesis of nanosized materials especially metal oxide nanostructures. After combining the O₂^{-•} anionic radicals with the AgI due to the presence of a strong interaction between them [AgOI] radicals may form. The [AgOI] radicals can react with the H⁺ ions, and OH radicals generate AgI and H₂O on the surface of TiO₂ and graphene nanostructures.

4. Conclusion

AgI-TiO₂-G composite was prepared in the presence of ultrasound irradiation. The nanocomposites of AgI-TiO₂-G, TiO₂-G, and AgI-G and the hybrid of AgI-TiO₂ were analyzed by using XRD, FESEM, TEM, energy dispersive X-ray spectroscopy, DRS, and fourier-transform infrared spectroscopy. This ternary composite showed higher photocatalytic performance in photodegradation of AO7 than TiO₂-G, AgI-G, AgI-TiO₂, and bare AgI, TiO₂, and graphene. In order to investigate the presence of graphene, TiO₂ and AgI and three other composites (AgI-TiO₂, AgI-G, and TiO₂-G) were synthesized and their performance in AO7 photodegradation was compared with ternary composite. According to the results, 4 wt% TiO₂ and 50 wt% AgI nanoparticle-loaded graphene exhibited the optimum condition for photodegradation of AO7 dye. Significant enhancement in the photodegradation efficiency was obtained from the graphene, which possesses good dye adsorptivity, high carrier transportation, and effective charge carrier separation properties. In addition to evaluating the effect of graphene, the impact of other parameters such as ultrasound irradiation and weight ratios of TiO₂ to graphene and AgI to graphene were investigated.

Acknowledgement

Authors are grateful to Council of University of Tehran for providing financial support to undertake this work.

References

- [1] J. Shen, Y. Hu, M. Shi, N. Li, H. Ma, M. Ye, One step synthesis of graphene oxide-magnetic nanoparticle composite, *J. Phys. Chem.*, 114 (2010) 1498–1503.
- [2] A.K. Geim, K.S. Novoselov, The rise of graphene, *Nat. Mater.*, 6 (2007) 183–191.
- [3] V. Singh, D. Joung, L. Zhai, S. Das, S. Khondaker, S. Seal, Graphene based materials: past, present and future, *Mater. Sci.*, 56 (8) (2011) 1178–1271.
- [4] F. Tavakoli, M. Salavati Niasari, A facile synthesis of Cu/graphene nanocomposite by glucose as a green capping agent and reductant, *J. Ind. Eng. Chem.*, 20 (2014) 3170–3174.
- [5] M. Salavati Niasari, F. Tavakoli, Pb(OH)I-graphene composite: synthesis and characterization, *J. Ind. Eng. Chem.*, 21 (2015) 1208–1213.
- [6] G. Shiravand, A. Badiei, G. Mohammadi Ziarani, M. Jafarabadi, M. Hamzehloo, Photocatalytic synthesis of phenol by direct hydroxylation of benzene by a modified nanoporous silica (LUS-1) under sunlight, *Chin. J. Catal.*, 33 (2012) 1347–1353.
- [7] H. Eskandarloo, A. Badiei, M.A. Behnajadi, G.M. Ziarani, Ultrasonic-assisted degradation of phenazopyridine with a combination of Sm-doped ZnO nanoparticles and inorganic oxidants, *Ultrason. Sonochem.*, 28 (2016) 169–177.
- [8] H. Eskandarloo, A. Badiei, M.A. Behnajadi, A. Tavakoli, G.M. Ziarani, Ultrasonic-assisted synthesis of Ce doped cubic-hexagonal ZnTiO₃ with highly efficient sonocatalytic activity, *Ultrason. Sonochem.*, 29 (2016) 258–269.
- [9] A. Fujishima, X. Zhang, D.A. Tryk, TiO₂ photocatalysis and related surface phenomena, *Surf. Sci.*, 63 (2008) 515–582.
- [10] K. Hashimoto, H. Irie, A. Fujishima, TiO₂ photocatalysis: a historical overview and future prospects, *Jpn. J. Appl. Phys.*, 44 (2005) 8269–8285.
- [11] S. Malato, P. Fernández-Ibáñez, M.I. Maldonado, J. Blanco, W. Gernjak, Decontamination and disinfection of water by solar photocatalysis: recent overview and trends, *Catal. Today*, 147 (2009) 1–59.
- [12] S. Escobedo, B. Serrano, A. Calzada, J. Moreira, H.D. Lasa, Hydrogen production using a platinum modified TiO₂ photocatalyst and an organic scavenger, *Kinetic modeling, Fuel*, 181 (2016) 438–449.
- [13] I.V. Lightcap, T.H. Kosel, P.V. Kamat, Anchoring semiconductor and metal nanoparticles on a two-dimensional catalyst mat. Storing and shuttling electrons with reduced graphene oxide, *Nano Lett.*, 10 (2010) 577.
- [14] H. Zhang, X.J. Lv, Y.M. Li, Y. Wang, J.H. Li, P25-graphene composite as a high performance photocatalyst, *ACS Nano*, 4 (2010) 380–386.
- [15] Y.H. Zhang, Z.R. Tang, X.Z. Fu, Y.J. Xu, TiO₂ graphene nanocomposites for gas-phase photocatalytic degradation of volatile aromatic pollutant: is TiO₂-graphene truly different from other TiO₂-carbon composite materials, *ACS Nano*, 4 (2010) 7303–7314.
- [16] Y. Liang, H. Wang, H.S. Casalongue, Z. Chen, H. Dai, TiO₂ nanocrystals grown on graphene as advanced photocatalytic hybrid materials, *Nano Res.*, 3 (2010) 701–705.
- [17] B. Cai, J. Wang, S. Gan, D. Han, Z. Wu, L. Niu, A distinctive red Ag/AgCl photocatalyst with efficient photocatalytic oxidative and reductive activities, *J. Mater. Chem. A.*, 2 (2014) 5280–5286.
- [18] Q. Wang, M. Chen, N. Zhu, X. Shi, H. Jin, Y. Zhang, Y. Cong, Preparation of AgI sensitized amorphous TiO₂ as novel high-performance photocatalyst for environmental applications, *J. Colloid Interface Sci.*, 448 (2015) 407–416.
- [19] X.Y. Zhang, H.P. Li, X.L. Cui, Y.H. Lin, Graphene-TiO₂ nanocomposites: synthesis, characterization and application in hydrogen evolution from water photocatalytic splitting, *J. Mater. Chem.*, 20 (2010) 2801–2806.
- [20] F. Tavakoli, M. Salavati-Niasari, F. Mohandes, Sonochemical synthesis and characterization of lead iodide hydroxide micro/nanostructures, *Ultrason. Sonochem.*, 21 (2014) 234–241.
- [21] F. Mohandes, M. Salavati-Niasari, Sonochemical synthesis of silver vanadium oxide micro/nanorods: solvent and surfactant effects, *Ultrason. Sonochem.*, 20 (2013) 354–365.
- [22] X. Lin, J. Xing, W. Wang, Z. Shan, F. Xu, F. Huang, Photocatalytic activities of heterojunction semiconductors Bi₂O₃/BaTiO₃: a strategy for the design of efficient combined photocatalysts, *J. Phys. Chem. C.*, 111 (2007) 18288–18293.
- [23] B. Neppolian, A. Bruno, C.L. Bianchi, M. Ashokkumar, Graphene oxide based Pt-TiO₂ photocatalyst: ultrasound assisted synthesis, characterization and catalytic efficiency, *Ultrason. Sonochem.*, 19 (2012) 9–15.
- [24] H. Eskandarloo, A. Badiei, M.A. Behnajadi, G. Mohammadi Ziarani, Ultrasonic-assisted sol-gel synthesis of samarium, cerium co-doped TiO₂ nanoparticles with enhanced sonocatalytic efficiency, *Ultrason. Sonochem.*, 26 (2015) 281–292.
- [25] H. Eskandarloo, A. Badiei, A.R. Tavakoli, M.A. Behnajady, G. Mohammadi Ziarani, Simple and safe educational experiments for demonstration of environmental application of heterogeneous photocatalysis process using the example of

- natural fruit juice dye degradation, *J. Mater. Educ.*, 36 (2014) 111–116.
- [26] H. Eskandarloo, A. Badiei, C. Haug, Enhanced photocatalytic degradation of an azo textile dye by using TiO₂/NiO coupled nanoparticles: optimization of synthesis and operational key factors, *Mater. Sci. Semicond. Process.*, 27 (2014) 240–253.
- [27] Q. Huang, S. Tian, D. Zeng, X. Wang, W. Song, Y. Li, W. Xiao, C. Xie, Enhanced photocatalytic activity of chemically bonded TiO₂/graphene composites based on the effective interfacial charge transfer through the C–Ti bond, *ACS Catal.*, 3 (2013) 1477–1485.
- [28] L. Chen, D. Jiang, T. He, Z. Wu, M. Chen, In-situ ion exchange synthesis of hierarchical AgI/BiOI microsphere photocatalyst with enhanced photocatalytic properties, *Cryst. Eng. Commun.*, 15 (2013) 7556–7563.
- [29] Y. Zhang, Z.R. Tang, X. Fu, Y.J. Xu, TiO₂-graphene nanocomposites for gas-phase photocatalytic degradation of volatile aromatic pollutant: is TiO₂-graphene truly different from other TiO₂-carbon composite materials?, *ACS Nano*, 4 (2010) 7303–7314.
- [30] S.D. Perera, R.G. Mariano, K. Vu, N. Nour, O. Seitz, Y. Chabal, K.J. Balkus, Hydrothermal synthesis of graphene-TiO₂ nanotube composites with enhanced photocatalytic activity, *ACS Catal.*, 2 (2012) 949–956.
- [31] Z. Li, M. Qi, C. Tu, W. Wang, J. Chen, A. JunWang, Highly efficient removal of chlorotetracycline from aqueous solution using graphene oxide/TiO₂ composite: properties and mechanism, *Appl. Surf. Sci.*, 425 (2017) 765–775.
- [32] K. Lv, S. Fang, L. Si, Y. Xia, W. Ho, M. Li, Fabrication of TiO₂ nanorod assembly grafted rGO (rGO@TiO₂-NR) hybridized flake-like photocatalyst, *Appl. Surf. Sci.*, 391 (2017) 218–227.
- [33] Q. Xiang, J. Yu, M. Jaroniec, Enhanced photocatalytic H₂-production activity of graphene-modified titania nanosheets, *Nanoscale*, 3 (2011) 3670–3678.
- [34] Q. Xiang, J. Yu, M. Jaroniec, Graphene-based semiconductor photocatalysts, *Chem. Soc. Rev.*, 41 (2012) 782–796.
- [35] M. Sabet, M. Salavati-Niasari, Deposition of lead sulfide nanostructure films on TiO₂ surface via different chemical methods due to improving dye-sensitized solar cells efficiency, *Electrochim. Acta*, 169 (2015) 168–179.
- [36] F. Sangsefidi, M. Sabet, M. Salavati-Niasari, Synthesis and characterization of ceria nanostructures with different morphologies via a simple thermal decompose method with different cerium complexes and investigation the photocatalytic activity, *J. Mater. Sci. - Mater. Electron.*, 27 (2016) 8793–8801.